AFRL-OSR-VA-TR-2013-0523

(YIP 10) - MAGNETOPLASMONIC NANOMATERIALS - A ROUTE TO PREDICTIVE PHOTOCATALYTIC, LIGHT-HARVESTING AND FERROFLUIDIC PROPERTIES

KENNETH KNAPPENBERGER

FLORIDA STATE UNIVERSITY, THE

10/01/2013
Final Report

AIR FORCE RESEARCH LABORATORY
AF OFFICE OF SCIENTIFIC RESEARCH (AFOSR)/RSA
ARLINGTON, VIRGINIA 22203
AIR FORCE MATERIEL COMMAND

REPORT DOCUMENTATION PAGE

Form Approved
OMB No. 0704-0188

1. REPORT DATE *(DD-MM-YYYY)*	**2. REPORT TYPE**	**3. DATES COVERED** *(From - To)*
30-09-2013	Final Technical Report	15-06-2010 - 14-06-2013

4. TITLE AND SUBTITLE

Magnetoplasmonic Nanomaterials: A Route to Predictive Photocatalytic, Light - Harvesting and Ferrofluidic Properties

5a. CONTRACT NUMBER

5b. GRANT NUMBER
FA9550-10-1-0300

5c. PROGRAM ELEMENT NUMBER

6. AUTHOR(S)

Kenneth L. Knappenberger, Jr

5d. PROJECT NUMBER

5e. TASK NUMBER

5f. WORK UNIT NUMBER

7. PERFORMING ORGANIZATION NAME(S) AND ADDRESS(ES)

Florida State University
874 Traditions Way, 3rd Floor
Tallahassee, FL 32306-4166

8. PERFORMING ORGANIZATION REPORT NUMBER

9. SPONSORING / MONITORING AGENCY NAME(S) AND ADDRESS(ES)

USAF, AFRL, AFOSR
875 N. Randolph Street, Room 3112
Arlington, VA 22203

10. SPONSOR/MONITOR'S ACRONYM(S)

AFOSR

11. SPONSOR/MONITOR'S REPORT NUMBER(S)

12. DISTRIBUTION / AVAILABILITY STATEMENT

Unclassified Unlimited

13. SUPPLEMENTARY NOTES

14. ABSTRACT

Nanostructured materials offer great potential for utilization, storage, and transport of energy over much of the solar spectrum. These unique opportunities arise because nanomaterials often display strikingly different chemical and physical properties than their bulk counterparts. Under AFOSR support, my research group has provided structure-specific descriptions of the optical and electronic properties of nanoscale materials via the development and utilization of advanced spectroscopy techniques. Our advances encompass three main areas: 1) spectroscopy and applications of plasmon-supporting metal nanostructures, 2) optical properties of light-harvesting nanoparticle networks, and 3) development of new laser-based measurement techniques.

My group developed and used femtosecond plasmon resonance spectroscopy to study coherent electron dynamics in noble metal nanoparticles. We extensively studied hollow, fluid-filled gold nanospheres (HGN). Interest in these structures is multifold, but it stems primarily from size-dependent contributions to the localized surface plasmon resonance (LSPR) spectral position and line width. We found that the hollow morphology increases LSPR sensitivity to the surroundings. We are currently using this effect to study molecular dynamics at nanoparticle surfaces and in confined, nanoscale volumes.

We also described inter-particle electromagnetic coupling effects in plasmonic nanoparticle networks. We developed new

15. SUBJECT TERMS

16. SECURITY CLASSIFICATION OF:			**17. LIMITATION OF ABSTRACT**	**18. NUMBER OF PAGES**	**19a. NAME OF RESPONSIBLE PERSON**
a. REPORT	**b. ABSTRACT**	**c. THIS PAGE**			**19b. TELEPHONE NUMBER** *(include area code)*

Summary of Accomplishments

Nanostructured materials offer great potential for utilization, storage, and transport of energy over much of the solar spectrum. These unique opportunities arise because nanomaterials often display strikingly different chemical and physical properties than their bulk counterparts. Under AFOSR award #FA9550-10-1-300, we provided descriptions for the structure-specific optical and electronic properties of nanoscale materials. Advances were made, in part, through the development and utilization of advanced spectroscopy techniques. Our findings are published in seventeen peer-reviewed manuscripts, and my group is currently contracted to write three review articles highlighting our AFOSR-supported work. Accomplishments were made in three main areas:

1. Optical properties and electron dynamics of light-harvesting nanoparticle networks
2. Energy relaxation in plasmonic nanostructures
3. Development of new femtosecond laser-based spectroscopy techniques.

1. **Optical properties and electron dynamics of light-harvesting nanoparticle networks:** Our work on nanoparticle networks has included assemblies of both plasmonic metal nanoparticles and semiconducting nanocrystals.[1-9] When multiple metal nanoparticles are arranged into networks with small inter-particle gaps, optical excitation results in near-field coupling that significantly amplifies incident electromagnetic waves. Both the electric and magnetic field components can be amplified by this antenna effect, providing numerous opportunities for enhancing light-matter interactions relevant to solar energy conversion and negative index materials. Our research has focused on describing the optical properties of electromagnetically coupled gold nanoparticles. We have been especially active in developing and using nonlinear optical techniques to elucidate the electric- *and* magnetic-dipolar contributions to nanoparticle hyperpolarizabilities.[6,8,9] Recently, we have extended our experimental repertoire to include 3-D electron tomography for studying the influence of interfacial structure on the optical properties of plasmonic networks.[5]

In contrast to metals, optical excitation of semiconductors results in the formation of a bound electron-hole pair, or exciton. Inter-particle exciton energy transfer can result when nanocrystals are placed in close proximity. Because the exciton energy can be controlled synthetically, nanocrystals of different sizes can be arranged in a network to produce an optical (energetic) gradient, which allows for directional energy transfer from donating to accepting nanocrystals. My group uses magneto-optical spectroscopy to quantify state-resolved energy transfer efficiencies in semiconducting networks.[4,7,10]

Our most important AFOSR-supported achievements in the area of nanoparticle networks are: (a) descriptions of inter-particle plasmon modes for assemblies of hollow gold nanospheres, (b) size-dependent quantification of quadratic polarizabilities for hollow nanospheres, (c) the first quantification of the electric- and magnetic-dipolar contributions to the nonlinear optical response of colloidal nanoparticle networks, (d) detailed studies of state-resolved inter-particle energy transfer efficiency for semiconducting nanocrystal assemblies, and (e) the use of selective spatial confinement of exciton fine-structure states and sample orientation in 1-D nanocrystals to manipulate nanorod optical properties.

2. Energy relaxation in plasmonic nanostructures: Metal nanoparticles with dimensions exceeding a few nanometers are most accurately described as a Fermi gas, and they exhibit localized surface plasmon resonance (LSPR) excitations. Because of LSPR phenomena, excitation of metal nanoparticles produces large local surface fields at structure-specific frequencies, allowing plasmonic nanoparticles to function as electromagnetic antennas. This light amplification can be exploited to increase optical signals and facilitate solar energy conversion. LSPR surface fields decay rapidly into the surroundings and exhibit plasmon mode frequency shifts due to variations in the local refractive index. As such, these materials can also function as sensors. Our AFOSR-supported research utilizes femtosecond pump-LSPR probe spectroscopy to understand the influence of nanoparticle morphology on electronic energy relaxation, and, in turn, plasmon sensitivity to environmental changes.[11-14] In continuing research, we are describing the optical and electronic properties of nanometals in the range of sizes from 1 nm to 2 nm. The transformation from the Superatom properties of nanoclusters to the metallic behavior of nanoparticles appears to occur on this size scale. The importance of understanding size-dependent electronic structure is reinforced by the discovery of catalysis by nanoclusters. Rapid progress in size-selective colloidal synthesis of ligand-protected nanoclusters has provided an avenue for obtaining a better understanding of size-dependent optical and electronic properties. Our research focuses on the examination of electronic relaxation dynamics using femtosecond time-resolved and magneto-optical spectroscopy methods, with a goal of providing improved size-dependent correlations for nanocluster optical properties. Our most important achievements in this area are: (a) detailed studies of electronic energy relaxation in hollow plasmonic nanostructures, (b) analysis of the LSPR line width response to changes in the interfacial dielectric of nanoscale materials, (c) size-dependent acoustic modes of hollow and solid metal nanostructures, and (d) quantification of thermodynamic properties for fluids confined to nanoscale volumes.

3. **Development of new femtosecond laser-based spectroscopy techniques:** Continued progress toward understanding the optical and electronic properties of nanoscale materials requires the development and implementation of advanced spectroscopy techniques. My group has been very active in this area, providing advances in time-resolved magneto-optical spectroscopy, improvements to the spatial accuracy of nanoparticle-based nonlinear optical imaging, and quantitative use of polarization-resolved second order nonlinear optical spectroscopy.

Specific Outcomes

1. Optical properties and electron dynamics of light-harvesting nanoparticle networks.

1.a. Plasmonic Metal Nanoparticle Networks. We have been very active in describing inter-particle electromagnetic coupling effects in plasmonic dimers and small aggregates. This work has been published in the *Journal of the American Chemical Society, Journal of Physical Chemistry Letters*, *Journal of Physical Chemistry C,* and *Physical Chemistry Chemical Physics*. We have studied a comprehensive range of hollow gold nanospheres (HGNs) ranging from 30 nm / 8 nm (outer diameter/shell thickness) to 52 nm / 4 nm, having aspect ratios spanning 3.5 to 11.7.[2] Using systematic variation within this range, we investigated the effects of particle aspect ratio, inter-particle gap size, and nanosphere inner surface spatial separation on the frequency of

hybridized LSPR resonances of HGN assemblies. We showed that altering these properties in aggregated HGNs led to control over the inter-particle plasmon resonance.[2] Thiol-mediated aggregation was accomplished using either ethane dithiol or cysteine, resulting in dimeric structures in which monomer subunits were spatially separated by < 3 Å or 1.2 ± 0.7 nm, respectively. Particle dimensions and separation distances were confirmed by TEM. Experimental extinction spectra obtained for high-aspect ratio nanospheres dimerized using ethane dithiol exhibited an obvious blue shift of the LSPR resonance relative to that observed for the native, monomeric HGN.[2] The exact cause of the blue shifting remains an open question, but several factors may play key roles: (1) significant coupling contributions from high-order multipolar modes (e.g. quadrupolar mode), (2) increased effects of higher-energy antibonding modes, or (3) formation of a charge-transfer plasmon resonance involving the cavity modes. The extent of the blue shift was dependent upon shell thickness: dimers comprised of thin-shelled HGNs exhibited the largest shift; aggregates containing HGNs with thick shells (≥ 7 nm) did not display a significant LSPR shift when the individual particles were in contact. Our paper published in the *Journal of the American Chemical Society* was the first report of an aggregation-induced blue shift of a hollow nanosphere's LSPR.[2] Until this time, it was commonly held that nanosphere aggregation resulted in an LSPR red shift owing to dielectric screening. As a result of our work, several theoretical and experimental groups have become interested in describing this unique phenomenon. We detailed our findings that all cysteine-induced aggregates that we examined displayed large inter-particle gaps (>1 nm) and a red-shifted LSPR, regardless of particle dimensions.[2] This effect can be described fully by a surface-mode-coupling model. All experimental measurements were verified by finite-difference time-domain (FDTD) calculations. In addition, simulated electric field maps highlighted the importance of the inner HGN surface in the inter-particle coupling mechanism.

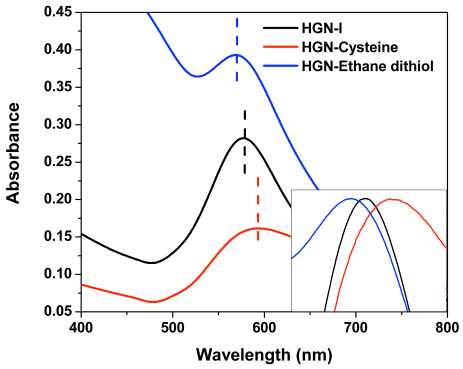

Figure 1. Experimental extinction spectra comparing isolated HGN (black) and HGN aggregates induced by ethane dithiol (blue) and dimerized cysteine (red). Truncated spectra (normalized at respective LSPR maxima) are shown in the inset to show more clearly the structure-dependent peak shifts. Originally published in reference 2.

Experimental determination of the origin of inter-particle plasmon resonances of complex structures, like the blue shifting observed for high-aspect ratio HGNs, necessitates the use of an optical single-particle technique that is highly sensitive to both the amplitude and polarization of the local electric field of the HGN dimer plasmons. Nonlinear optical (NLO) microscopy measurements combined with single-particle detection provide much more information than linear optical techniques for this purpose. For example, the input polarization dependence of the Second Harmonic Generation (SHG) signal intensities distinguishes whether dipolar or higher-order multipolar (i.e. quadrupolar) contributions are responsible for the observed inter-particle plasmon resonances of nanoparticle assemblies (to be published). In the SHG technique (a second-order process), two photons at the fundamental laser frequency (ω) are converted into one photon at the harmonic frequency (2ω). During the AFOSR-funding period, we built a

single-particle microscope based on SHG, which is highly sensitive to the amplitude and polarization of the electric field as well as the structure of the material. Also, we have shown the Complete Polarization Variation-Second Harmonic Generation (CPV-SHG) technique can be used to quantify the relative contributions from electric and magnetic dipoles to the nonlinear optical response of electromagnetically coupled colloidal nanoparticles.[6,8,9]

First, we reported the optical quadratic nonlinearity of hollow gold nanospheres (HGNs) in the *Journal of Physical Chemistry C* (**2010**, *114*, 19971).[3] We used the Two-Photon Rayleigh Scattering (TPRS) technique to measure the first hyperpolarizabilities (β) of these nanospheres. The measured β values were extremely large for the HGNs and, more interestingly, larger than similarly sized solid gold nanospheres (SGNs). Moreover, the β value could be tuned by varying the size of the HGNs. The augmentation of HGN β values relative to those observed for SGNs resulted, in part, from larger surface area, local electromagnetic field enhancement arising from surface morphology, and one-photon resonance enhancements observed for large- aspect-ratio structures with near-infrared surface-plasmon resonances. For HGN aggregates, the TPRS response depended strongly upon aggregate interfacial structure and the resulting inter-particle interaction mechanisms. This effect is shown in Figure 2. This finding illustrates the sensitivity of NLO techniques like TPRS for probing both nanoscale structure-dependent optical properties and the nature of inter-nanoparticle interactions. In addition, these nanostructures may prove valuable for single-particle detection and negative-index metamaterials. With the current interest in nanoparticle-based negative-index materials, the superior nonlinear optical performance we observed for HGNs may have a large impact.

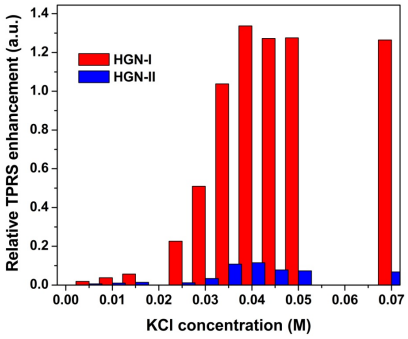

Figure 2. Relative Two-Photon Rayleigh Scattering response from different HGN samples, HGN-I (red) and HGN-II (blue), as a function of KCl-induced aggregation. Relative TPRS enhancement (Δ) has been determined as $\Delta = [I_{TPRS(aggregated)} - I_{TPRS(isolated)}]/ I_{TPRS(isolated)}$. A significant enhancement is observed for the HGN-I system. This effect resulted from structure-dependent LSPR frequencies.

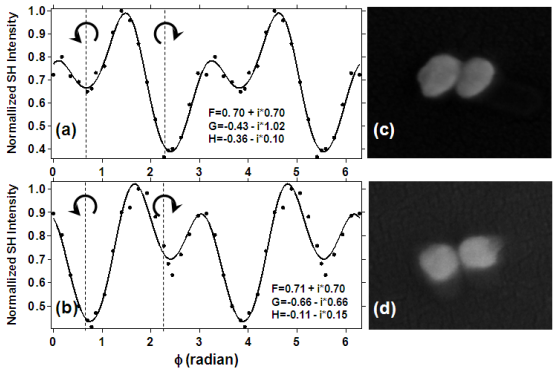

Figure 3. SHG line shapes obtained from Continuous Polarization Variation measurements on two different SGN dimers. Solid dots represent the experimental data, and the solid line is a fit to the data using an equation we described in JACS **2012**, *134*, 4477. Nonzero values of G reflect magnetic dipolar contributions to the signal. Polarization line shapes depicted in (a) and (b) were determined for the specific dimer structures shown in images (c) and (d), respectively.

Using our home-built SHG microscope, we quantified both the relative electric-dipolar and magnetic-dipolar contributions to the plasmon-mediated nonlinear optical response of dimeric solid gold nanospheres.[6,8,9] Quantitative analysis of the complex-valued tensorial components was made possible by measuring the complete polarization dependence of the SHG

signal obtained from plasmonic structures at the single-particle level, as is shown in Fig. 3 and described in the *Journal of the American Chemical Society* **2012**, *134*, 4477. Based on these data, we determined that the relative electric- and magnetic-dipolar contributions were both structure dependent and unique to each nanoparticle assembly; polarization-resolved measurements suggested electric-quadrupolar moments were not important for this nanoparticle size. This work indicates that metal nanoparticle networks can be used as both electric and magnetic field transducers upon optical excitation, resulting in localized magnetic fields. In continuing research, my group is exploiting this plasmon amplification to develop spatially resolved spectroscopy methods, including magneto-optical [e.g. magnetic circular dichroism (MCD)] techniques. Because MCD is inherently sensitive to oxidation and spin state, we will be able to use this technique in the future to study interfacial charge transfer and photocatalysis at nanoparticle surfaces. To do so, we will extend the NLO imaging platform developed under AFOSR support to include temporal and improved spatial accuracy.

Currently, my group is very active in using plasmon amplification to increase the spatial accuracy of nonlinear optical spectroscopy/imaging techniques. Optical microscopy is an indispensible tool for constructing images of heterogeneous chemical environments and complex materials. A major advantage of NLO imaging is that the input wave parameters can be tailored to generate chemical- and material-specific signals. Although imaging resolution is diffraction limited, the position of a point-source signal can be determined with high accuracy, limited primarily by signal strength. In a related project, we have shown that NLO enhancement by electromagnetically coupled plasmonic nanoparticles yields images acquired with high temporal resolution (2 frames per second) and a localization accuracy of one nanometer, published in the Journal of Chemical Physics. My group will utilize this method, along with magneto-optical spectroscopy, to study molecular dynamics at nanoparticle surfaces.

1.b. Semiconducting Nanoparticle Networks. My group has made significant advances in the spectroscopy, synthesis and characterization of light-harvesting semiconducting nanocrystals.[1,4,7] As part of this effort, we have formed multi-layer structures that function in the visible spectral region, as well as assemblies of nanocrystals that absorb in the NIR. In the latter case, we developed a new low-temperature synthesis (*Langmuir* **2010**, *25*, 10636) for mercury telluride (HgTe) quantum dots (QDs) using generation-5 (G5) and -7 (G7) polyamidoamine (PAMAM) dendrimers, which function both as nucleation sites and nanoparticle stabilizers. Absorption maxima for HgTe QDs ranged from 950 to 970 nm, depending on the dendrimer generation and concentration. We showed that we could optimize the QD size distribution by careful variation of the molar ratio of Hg^{2+} to dendrimer surface groups for both G5 and G7 dendrimers. An increase in molar ratio from 1:0.5 to 1:4 resulted

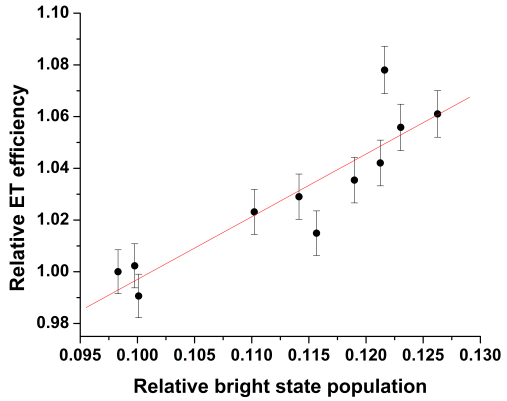

Figure 4. Calculated energy transfer efficiency as a function the relative population of the "bright" state of the energy-donating nanocrystal within the CdSe assemblies. The red line demonstrates the linear relationship between the two parameters.

in a decrease in the half width at half maximum (HWHM) of the HgTe bandgap absorption from 68±3 nm to 52±2 nm, indicating a size distribution focusing of 23±4%. Second derivative analysis of HgTe QD FTIR absorption spectra suggested that the quantum dots were fully encapsulated by a single G7 dendrimer, whereas multiple G5 dendrimers were necessary to stabilize a single nanoparticle. TEM and FTIR data revealed that the HgTe QDs formed 2-D necklace-type arrays through a self-organization process, which proceeded via interpenetration of dendritic arms. TEM data further indicated that the average nano-necklace contained 10-15 QDs with an average inter-QD separation of 1.3±0.7 nm and a total chain length of 46±6 nm.

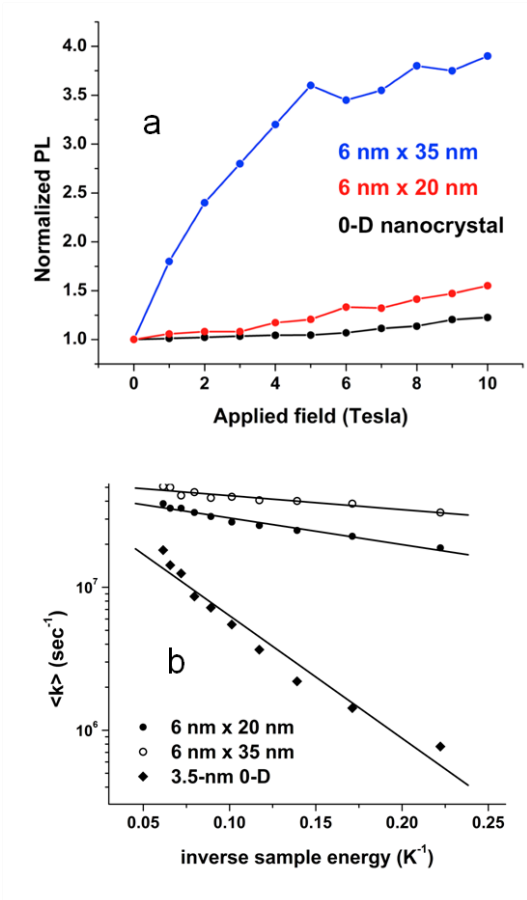

Figure 5. (a) Normalized magnetic-field dependent CdSe photoluminescence obtained from 3.5-nm 0-D quantum dots (black), 6 nm x 20 nm nanorods (red), and 6 nm x 35 nm nanorods following 400-nm excitation at 4.2 K. All data are normalized with respect to the zero-field integrated intensity. (b) Arrhenius analysis of CdSe nanocrystal magneto-photoluminescence. The log-linear plot portrays the radiative rate constant as a function of the inverse of the sample energy. The slope reflects the energy gap separating the bright and dark exciton states. The data clearly reflected a larger bright-dark energy gap for nanocrystals with strong spatial confinement in three dimensions than for nanorods. Note: The 0-D data deviates from 1st-order behavior. This affect may be due to random field-sample orientations. Nonetheless, the size-dependent field sensitivities were clearly evident in the MPL data.

In order to study the optical properties and energy transfer efficiencies of light-harvesting nanocrystal assemblies, my group utilizes temperature-dependent, intensity-integrated and energy-resolved measurements in applied magnetic fields.[4,7,10] These measurements are especially informative because nanocrystal emission energies, amplitudes and polarizations all provide insight into competitive energy relaxation processes, such as radiative recombination, energy transfer, phonon coupling, and charge carrier trapping. By decreasing the sample temperature from 300 K to 6 K, we were able to suppress access to surface trap states and other thermal losses, resulting in a 3-fold photoluminescence intensity increase that was directly reflected in inter-particle energy transfer efficiency (*Phys.Chem.Chem.Phys.* **2012**, *14*, 11053). Using magneto-photoluminescence measurements we quantified the relative populations and energy separations of exciton fine structure states in energy-donating nanocrystals and determined their influence on energy transfer efficiency. In order to perform this analysis, we developed a method for determining the relative bright (J = ± 1) and dark (J = ± 2) fine-structure state populations (*J. Phys. Chem. C,* **2011**, *115*, 14517). Our results showed that energy transfer efficiency could be increased when the J = ± 1 fine structure state was selectively populated (Fig. 4). The experimental data indicated an energy transfer efficiency enhancement of

approximately 7%, which was limited by the random orientation of the crystalline c-axis of nanocrystals in light-harvesting assemblies. The orientation was limiting because the ability to manipulate the nanocrystal optical properties depends upon the angle formed by the incident magnetic field vector and the material crystalline c-axis.

As an extension of the initial work on spherical nanocrystals, we have used 1-dimensional nanorods to overcome the geometric limitations imposed by 0-D geometries. A manuscript detailing these findings has been published (*Nanoscal*e **2013**, *5*, 9049).[10] This manuscript was selected as a "hot paper" by the *Nanoscale* editorial board and featured on the journal home page. In this work, we showed that applied magnetic fields can be used to control the optical properties of semiconducting nanorods. We also demonstrated that the semiconductor aspect ratio, as well as the relative orientations of the applied field vector and the nanocrystal's c-axis, dictated the extent to which these properties could be controlled. This exciting development suggests that geometric control over the formation of extended nanostructure arrays can be used to tailor material optical properties, including vectorial energy transfer. In the 1-D system, application of magnetic fields led to enhancements of the emission efficiency that exceeded those observed for 0-D structures by a factor of four (Fig. 5a). These data also demonstrated the role of nanorod dimensions in determining MPL enhancement. Using temperature-dependent MPL measurements, we determined that the behaviors observed in Fig. 5a resulted from size-dependent energy separations between the J = ± 1 (bright) and J = ± 2 (dark) exciton states that resulted from different degrees of spatial confinement for the CdSe sp^3 conduction band wave functions, thus affecting the exchange interaction between the electron and hole states. The size dependence of these energy levels is clearly apparent in the first-order Arrhenius analysis shown in Fig. 5b. A cross over in the energy order of the exciton fine structure states was also observed. This cross over also resulted in the apparent observation of an Aharonov-Bohm phase shift that occurred when fields greater than 6T were applied orthogonal to the nanorod crystalline c-axis. This key finding helps to improve the understanding of the electronic structure of non-spherical nanocrystals and indicates the optical and electronic properties can be tailored by selective three-dimensional spatial confinement. Many of our advancements on the 1-D nanorod system resulted from the use of time-resolved magneto-optical measurements. We are currently using femtosecond time-resolved magneto-optical spectroscopy to study these materials.

Our use of magneto-optical spectroscopy has been well received. To date we have been contracted to write three review articles on the use of magneto-optical spectroscopy for studying nanoparticle optical properties and excited state dynamics.

2. Energy relaxation in plasmonic nanostructures.

Under AFOSR support, my research group has also been very active in studying electronic relaxation dynamics in plasmon-supporting metal nanoparticles. We have studied hollow, fluid-filled gold nanospheres (HGN) extensively. HGNs are synthesized by the galvanic replacement of cobalt nanoparticles with gold (III) salts, forming a thin shell that encapsulates fluids. Interest in these structures is multifold: LSPR tunability, fluid confinement to cavity diameters spanning 3 nm to 50 nm, and size-dependent contributions to the LSPR spectral position and line width. Findings from my research program have been published in the *Journal*

of the American Chemical Society, Physical Chemistry Chemical Physics, and Nano Letters, and most of these findings are summarized in an invited Perspective that was published in *Journal of Physical Chemistry Letters* in 2013. We have found that the hollow morphology significantly influences electronic relaxation dynamics in high-aspect ratio nanoparticles and increases LSPR sensitivity to the surroundings.

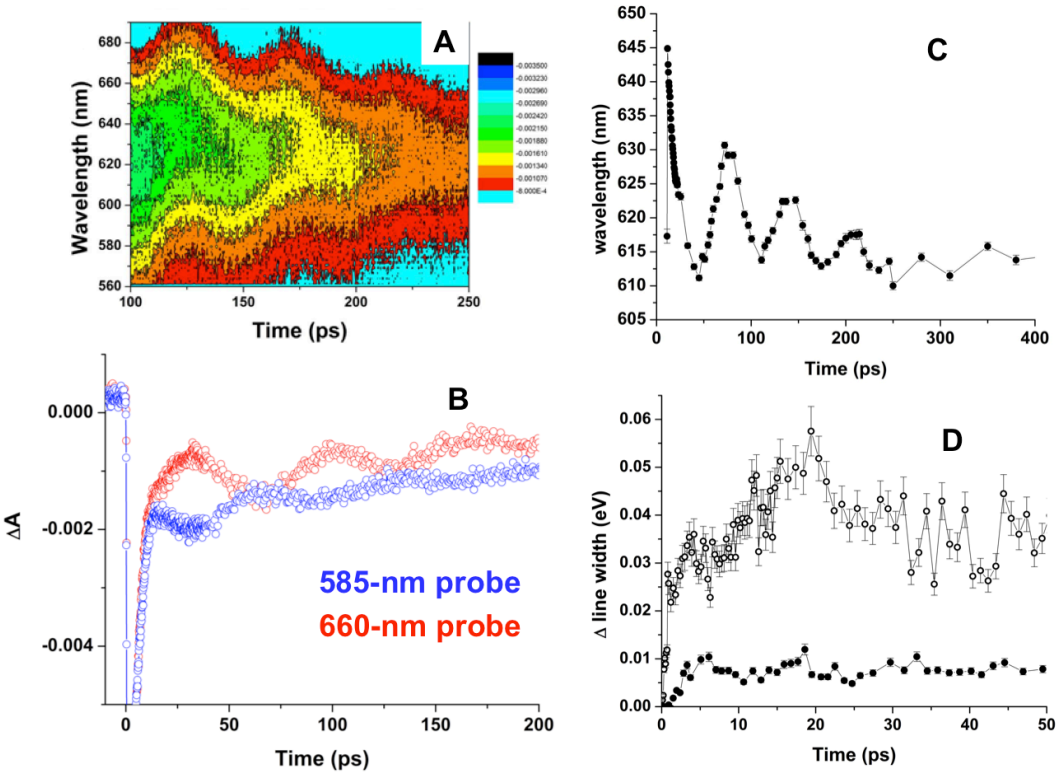

Figure 6. (A) Two-dimensional transient extinction image obtained for a hollow gold nanosphere following 400-nm excitation. (B) Transient extinction data obtained from the data in panel A by recording the differential amplitude at 585 nm (blue) and 660 nm (red). (C) Localized surface plasmon resonance central wavelength recorded as a function of pump-probe delay time. Taken together, these time-dependent data reflect changes in the nanoparticle volume and surrounding dielectric. (D) Comparison of the change in the LSPR line width for hollow (open circles) and solid (filled circles) nanospheres following excitation by a femtosecond laser pulse. The data in panel D demonstrate the enhanced sensitivity of hollow nanostructures to changes in interfacial dielectric induced by laser heating. Reprinted from reference 9.

In order to compare the sensitivities of HGN and SGN LSPRs to interfacial electron scattering, a series of femtosecond pump-surface plasmon resonance probe measurements were performed.[11] These experiments employ a broad bandwidth white-light continuum probe to monitor the LSPR at a controlled time delay following excitation by a femtosecond pump pulse. This technique is useful for studying relaxation dynamics of electronically excited metal nanostructures because it generates a non-equilibrium electron gas. As a result of this excitation, a transient bleach at the LSPR frequency features prominently in the differential pump-probe transient extinction spectra of metal nanoparticles. The hot electron gas relaxes by three successive steps: i) ultrafast electron-electron (e-e) scattering, ii) sub-picosecond electron-

phonon (e-ph) coupling, and iii) energy transfer from the hot nanoparticles to the surroundings on time scales spanning tens to several hundreds of picoseconds.[9] This rapid dissipation of electronic energy as heat to the surroundings modifies the dielectric constant of the embedding media, which in turn influences the interfacial scattering rate. Changes in local dielectric constants can be determined when data from femtosecond pump-surface plasmon resonance probe experiments are analyzed in both the time and energy domains. The large difference in the time scales of the local heating dynamics (10s of picoseconds) and plasmon dephasing (~10 fs) is key to the use of time-dependent modulations of the LSPR line width to study changes in the interfacial dielectric properties.[11] Because the plasmons dephase so rapidly, the local environment is essentially static during the plasmon coherence time, and spectroscopic measurements of the LSPR with femtosecond time resolution provide a snapshot of the local dielectric environment.

The wavelength-resolved transient extinction data obtained for HGNs with a 50-nm outer diameter is shown in Fig. 6a; the color represents the amplitude of the transient bleach. These data contain time-dependent modulations of the LSPR amplitudes, spectral position and peak width.[9,11] The observed modulations in the differential amplitude and spectral position resulted from differences in nanoparticle volume and local temperatures, respectively. As one example from our comprehensive study, the differential amplitude recorded at probe wavelengths of 585 nm (blue) and 660 nm (red) are plotted in Figure 6b. The oscillatory behavior shown in Figure 6b stemmed from laser-induced lattice expansion that caused a time-dependent alteration of the LSPR spectral position. This behavior is also apparent in Figure 6c, where the HGN center frequency is plotted as a function of pump-probe time delay. The time-dependent change in the LSPR line widths (reported in eV) derived from HGN and SGN data are compared in Figure 6d. The magnitude of the changes in the LSPR widths is greater for the HGN spectrum than for the SGN data (Figure 6d). Since the laser pulse energies are selected to achieve comparable heating conditions, observation of a larger line width change for HGNs than for SGNs indicates that the LSPR of HGNs is a more sensitive indicator of interfacial scattering, which results from modifications to the local dielectric. The results show significant advantages of hollow nanostructures over solid ones for interfacial/environmental sensing applications, especially for measurements carried out at the single-particle/molecule level.

Quantitative analysis of the intensity recurrences shown in Figure 6 provides insight into HGN coherent acoustic vibrations, which are important for predicting the mechanical properties of these materials. Fourier transformation of the coherent portion of the time domain data yields the frequency of the acoustic modes. We determined the frequencies for several particles.[11] Samples that have low aspect ratios exhibit a dominant mode with a frequency that is consistent with expectations based on isotropic lattice expansion of a solid nanosphere.[23] However, high-aspect-ratio (i.e. AR ≥ 0.65) HGNs have a single, low-frequency isotropic mode. This reduced frequency is attributed to mode softening arising from increased lattice polycrystallinity of HGNs with large surface-to-volume ratios.

To understand more fully the dependence of HGN acoustic modes on particle size, the coherent portions of the time-dependent extinction data were modeled using a damped sine function. This analysis reveals a π-phase shift between the high and low frequency modes.[28] This phase difference indicates a distinct mechanism for acoustic mode excitation. Specifically, lattice expansion of low-aspect ratio samples is launched via a direct mechanism, whereas acoustic modes are excited indirectly for large-aspect-ratio samples.[11] Direct excitation of the acoustic modes results from the electron pressure produced by laser-induced excitation of the non-

equilibrium electron gas.[11] In contrast, indirect excitation of acoustic modes dominates when electron-phonon equilibration is efficient, resulting in rapid heating of the metal lattice. The size-dependent transformation from direct to indirect excitation implies that electron-phonon coupling is more efficient for HGNs with a high surface-to-volume ratio - or that low aspect-ratio HGNs exhibit especially slow electron cooling rates. The latter effect could arise if HGN cavity dimensions influence interfacial thermal conductivities or if cavity-confined fluids have thermal effusivities that are distinct from bulk fluids. In order to study the size dependence of the electronic energy relaxation of HGNs, femtosecond time-resolved transient extinction data were collected for a range of particle sizes.[12] The electron-phonon equilibration, or coupling, rates can be quantitatively determined by monitoring the recovery kinetics of the LSRP transient bleach; the second step of the three-step electronic relaxation process described above provides a direct measure of electron-phonon coupling. Consistent with the observation that the mechanism for excitation of acoustic vibrational modes switches from direct to indirect as the aspect ratio of the HGN increases,[11] electron-phonon equilibration is accelerated for HGNs with larger aspect ratios and surface-to-volume ratios.[12] These findings suggest that the mechanical and optical properties of HGNs are, in part, determined by nanostructure dimensions.

We also quantified the thermal properties of the interface between HGNs and their surroundings using femtosecond time-resolved-LSPR probe spectroscopy. The energy relaxation data shown in Figure 7a demonstrate the unique ability of HGNs to inform on environmental properties. The nanoparticle-to-surroundings-energy-transfer half times obtained from transient extinction measurements are plotted as a function of HGN surface area. The data exhibit two distinct categories: 1) HGNs with cavity radii < 15 nm and 2) HGNs with cavity radii ≥ 15 nm.[13] In both cases, the relaxation half times are directly proportional to HGN surface area, and energy dissipation presents as heat transferred to the surroundings. The relative efficiencies of metal-to-surroundings energy transfer per unit volume, γ (fs/nm^2), were then compared for the large- and small-cavity HGN

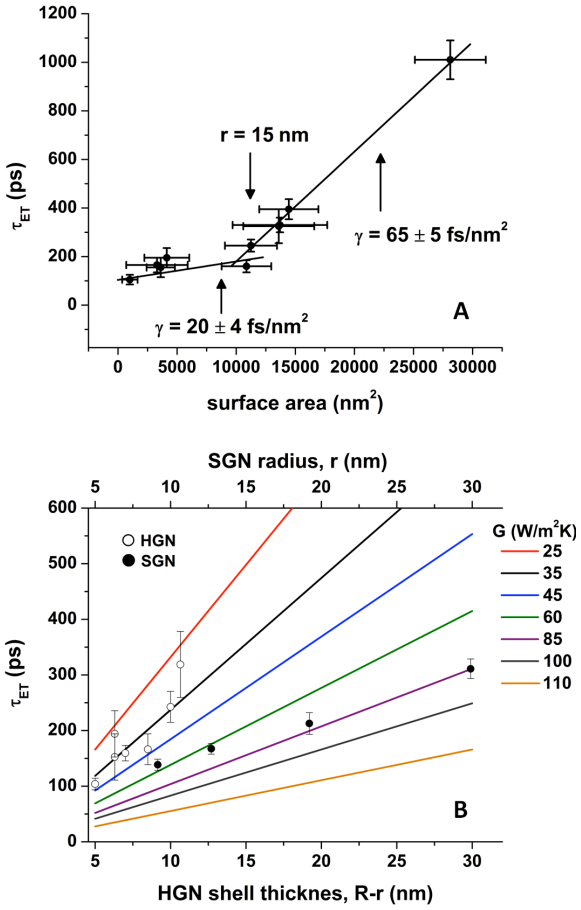

Figure 7. (A) Nanoparticle-to-surroundings energy transfer half times (τ_{ET}) of HGNs plotted as a function of their total surface area. These HGNs have cavity radii ranging from 3.3 to 27.5 nm. The data reflect a clear discontinuity in linear surface area dependence for cavity radii less that 15 nm. (B) HGN (open circles) and SGN (filled circles) energy transfer half times (τ_{ET}) plotted as a function of HGN shell thickness, or SGN radius. The experimental data are also poltted with calculated size-dependent interfacial thermal conductivities (colored lines). Originally published in reference 13.

regimes.[13] In the case of ≥ 15-nm cavity radii, $\gamma = 65 \pm 5$ fs/nm^2; these values are within error of those obtained for solid gold nanospheres ($\gamma = 62 \pm 3$ fs/nm^2). In contrast, analysis of the data for < 15-nm cavity radii yields $\gamma = 20 \pm 4$ fs/nm^2.[13] The data shown in Figure 7a lack HGN samples with cavity radii between 8 nm and 15 nm. Recent analysis suggests that the discontinuity in the relaxation data likely occurs when the HGN cavity radius reaches 8 nm rather than 15 nm. Therefore, the transformation between small- and large-cavity HGNs may in fact be smoother than the abrupt change reflected in Figure 7a. The observed size-dependent effects could be due to volume-dependent changes in the thermal conductivities of water, or to radius-dependent modifications to surface tension of the cavity-confined fluids. Additional experiments are needed to describe this phenomenon completely.

In addition to surface area, the energy relaxation rates are also influenced by the thermal effusivity of the surroundings. The obvious break in the data shown in Figure 7a indicates that the thermal properties of fluids confined to small cavity volumes are distinct from those of bulk fluids and those occupying larger cavities. Analysis of the nanoparticle/fluid interfacial thermal conductivity (G) provides insight into the volume-dependent thermal conductivity of confined fluids. Figure 7b shows a comparison of the experimentally derived values of G for HGNs with small cavity radii ≤ 8 nm (open circles) and SGNs (filled circles) to values calculated using the bulk thermal conductivity of water. The data indicate that the thermal conductivity of water confined to small cavities is approximately half that of bulk water.[13]

Together, the large surface-to-volume ratios of HGNs and the apparent influence of confined fluids play important roles in determining the relaxation dynamics of non-equilibrium electron gases generated by pulsed laser excitation. Understanding these fundamental processes is important for developing a predictive understanding of LSPR spectral positions, line widths and time-dependent modulations, which control transducer performance. Further, the combination of the plasmonic hollow nanosphere morphology, which confines fluids to nanoscale volumes, and the sensitivity of femtosecond pump-LSPR probe measurements to the local environment provides a unique experimental platform for understanding the thermal and dielectric properties of confined fluids. Insights from these studies will have broad applications because sequestration of small volumes of water is believed to mediate a diverse range of chemical and photocatalytic processes.

3. Development of new femtosecond laser-based spectroscopy techniques.

A significant component of my group's research efforts under AFOSR support involved the development of advanced magneto-optical and nonlinear optical spectroscopy techniques for studying nanoscale optical properties. As described previously, we developed single-particle Continuous Polarization Variation-Second Harmonic Generation (CPV-SHG) and spectroscopy to understand nonlinear optical properties of plasmonic nanoparticle networks, and we continue to be active in this area. We have also developed a nonlinear optical imaging platform capable of providing one-nanometer spatial accuracies (160x the diffraction limit). For semiconductor nanostructures, we implemented time-resolved magneto-photoluminescence measurements to study inter-particle energy transfer.

In our FSU lab we have developed femtosecond time-resolved magnetic circular dichroism (MCD) capabilities. MCD data are highly sensitive to the electronic structure of molecules and nanoclusters. In light of this, we currently employ time-resolved MCD to investigate the interplay between nanoscale structure and optical and electronic properties. Our

approach to building this instrument involves the utilization of an ultra-short circularly polarized continuum probe pulse. Generation of this light is a non-linear process, and, therefore, the seed pulse parameters were anticipated to affect the polarization properties of the continuum. Therefore, my research group developed the skills to control and characterize fully the polarization properties of broad bandwidth (continuum) laser pulses. To achieve control over these parameters, a spatial light modulator is utilized to adjust selectively the phase and amplitude of specific frequency components of the seed laser pulse. The synthesized pulses are analyzed using the frequency-resolved optical gating (FROG) technique. To date, we have performed measurements using circularly polarized laser probe pulses spanning 450 nm – 1500 nm, with typical instrument response functions of a few hundred femtoseconds (the best IRF we have achieved to date is 90 fs). These technical advances will be documented in a manuscript currently under preparation.

The combination of these nonlinear optical imaging and femtosecond time-resolved techniques provides my research group with the opportunity to carry out magneto-optical measurements at the limits of temporal resolution and spatial accuracy. As such, these advances have established our group as a uniquely capable and competitive spectroscopy program that is able to make significant contributions to understanding dynamics and optical properties of nanoscale materials, as well as other areas that can benefit from advanced spectroscopy. In continuing research, we are introducing a multi-pulse stimulated Raman data acquisition scheme that will allow us to carry out femtosecond time-resolved vibrational MCD measurements.

Research Productivity

My research group has published seventeen papers detailing our work under AFOSR grant # FA9550-10-1-0300, and three additional invited review articles are currently contracted.[1-17] Our work on nanoparticle electron dynamics and optical properties has been also recognized with the Young Investigator Award of the Inter-American Photochemical Society. Our work has also been disseminated as invited talks at multiple international symposia, national ACS, OSA and SPIE meetings, two Gordon Research Conferences, and several departmental seminars. In total, the work has been presented at 48 invited talks over the funding period, and members of my research group have contributed several conference papers.

References:

1) A. Priyam, D. E. Blumling, K. L. Knappenberger, Jr. "Synthesis, Characterization, and Self Organization of Dendrimer-Encapsulated HgTe Quantum Dots" *Langmuir*, **26**, 10636-10644 (2010).
2) M. Chandra, A. M. Dowgiallo, K. L. Knappenberger, Jr. "Controlled Plasmon Resonance Properties of Hollow Gold Nanosphere Aggregates" *Journal of the American Chemical Society*, **132**, 15782 (2010).
3) M. Chandra, A. M. Dowgiallo, K. L. Knappenberger, Jr. "Two-Photon Rayleigh Scattering from Isolated and Aggregated Hollow Gold Nanospheres" *Journal of Physical Chemistry C*, **114**, 19971 (2010).
4) D. E. Blumling, T. Tokumoto, S. McGill, K. L. Knappenberger, Jr. "Magneto-photoluminescence Properties of Colloidal CdSe Nanocrystal Aggregates" *Journal of Physical Chemistry C*, **115**, 14517-14525 (2011).
5) S. M. Stagg, K. L. Knappenberger, Jr., A. M. Dowgiallo, M. Chandra "Three-Dimensional Interfacial Structure Determination of Hollow Gold Nanosphere Aggregates" *Journal of Physical Chemistry Letters*, **23**, 2946-2950 (2011).
6) M. Chandra, A. M. Dowgiallo, K. L. Knappenberger, Jr. "Magnetic Dipolar Interactions in Solid Gold Nanosphere Dimers" *Journal of the American Chemical Society*, **134**, 4477-4480 (2012).
7) D. E. Blumling, T. Tokumoto, S. McGill, K.L. Knappenberger, Jr. "Temperature- and Field- Dependent Energy Transfer in CdSe Nanocrystal Aggregates Studied by Magneto-photoluminescence Spectroscopy" *Physical Chemistry Chemical Physics*, **14**, 11051-11059 (2012).
8) M. Chandra and K. L. Knappenberger, Jr. "Nanoparticle Surface Electromagnetic Fields Studied by Single-Particle Nonlinear Optical Spectroscopy" *Physical Chemistry Chemical Physics* **15**, 4177-4182 (2013).
9) K. L. Knappenberger, Jr., A. M. Dowgiallo, M. Chandra and J. W. Jarrett "Probing the Structure-Property Interplay of Plasmonic Nanoparticle Transducers Using Femtosecond Laser Spectroscopy" *Journal of Physical Chemistry Letters*, **4**, 1109-1119 (2013).
10) D. E. Blumling, S. McGill and K. L. Knappenberger, Jr. "The Influence of Applied Magnetic Fields on the Optical Properties of Zero- and One-Dimensional CdSe Nanocrystals" *Nanoscale*, **5**, 9049-9056 (2013).
11) A. M. Dowgiallo, A. M. Schwartzberg, K. L. Knappenberger, Jr. "Structure-dependent Coherent Acoustic Vibrations of Hollow Gold Nanospheres" *Nano Letters*, **11**, 3258 (2011).
12) A. M. Dowgiallo, K. L. Knappenberger, Jr. "Ultrafast Electron-Phonon Coupling in Hollow Gold Nanospheres" *Physical Chemistry Chemical Physics*, **13**, 21585-21592 (2011).
13) A. M. Dowgiallo and K. L. Knappenberger, Jr. "Influence of Confined Fluids on Nanoparticle-to-Surroundings Energy Transfer" *Journal of the American Chemical Society*, **134**, 19393-19400 (2012).
14) D. Wheeler, T. D. Green, H. Wang, C. Fernandez-Lopez, L. Liz-Marzan, S. Zou, K. L. Knappenberger, Jr., J. Z. Zhang "Optical Properties and Coherent Vibrational Oscillations of Gold Nanostars" *Chemical Physics Letters*, **543**, 127-132 (2012).

15) X. Ji, G. Palui, T. Avellini, H. B. Na, C. Yi, K. L. Knappenberger, Jr., H. Mattoussi, "On the pH- dependent Quenching of Quantum Dot Photoluminescence by Redox Active Dopamine" *Journal of the American Chemical Society*, **134**, 6006-6017 (2012).
16) L. Guocan, K. Hu, C. Yi, K. L. Knappenberger, Jr., G. J. Meyer, S. I. Gorelsky and M. Shatruk "Panchromatic Light Harvesting and Hot Electron Injection by Ru(II) Dipyrrinates on TiO_2 Surface" *Journal of Physical Chemistry C*, **117** 17399-17411 (2013).
17) A. R. Attar, D. E. Blumling, K. L. Knappenberger, Jr. "Photodissociation of thioglycolic acid studied by femtosecond time-resolved transient absorption spectroscopy" *Journal of Chemical Physics*, **134**, 0254514 (2011).